International Journal of Extreme Manufacturing

TOPICAL REVIEW • OPEN ACCESS

The recent development of soft x-ray interference lithography in SSRF

To cite this article: Jun Zhao *et al* 2020 *Int. J. Extrem. Manuf.* **2** 012005

View the article online for updates and enhancements.

This content was downloaded from IP address 118.123.172.211 on 27/02/2020 at 02:21

OPEN ACCESS
IOP Publishing | IMMT International Journal of Extreme Manufacturing

Int. J. Extrem. Manuf. 2 (2020) 012005 (7pp) https://doi.org/10.1088/2631-7990/ab70ae

Topical Review

The recent development of soft x-ray interference lithography in SSRF

Jun Zhao[1,2], **Shumin Yang**[1,2], **Chaofan Xue**[1,2], **Liansheng Wang**[1,2], **Zhaofeng Liang**[1], **Lei Zhang**[2], **Yong Wang**[1,2], **Yanqing Wu**[1,2,3] and **Renzhong Tai**[1,2,3]

[1] Shanghai Synchrotron Radiation Facility, Shanghai Advanced Research Institute, CAS, Shanghai, People's Republic of China
[2] Shanghai Institute of Applied Physical, CAS, Shanghai, People's Republic of China

E-mail: wuyanqing@sinap.ac.cn and tairenzhong@sinap.ac.cn

Received 3 December 2019, revised 15 January 2020
Accepted for publication 21 January 2020
Published 26 February 2020

Abstract

This paper introduces the recent progress in methodologies and their related applications based on the soft x-ray interference lithography beamline in the Shanghai synchrotron radiation facility. Dual-beam, multibeam interference lithography and Talbot lithography have been adopted as basic methods in the beamline. To improve the experimental performance, a precise real-time vibration evaluation system has been established; and the lithography stability has been greatly improved. In order to meet the demands for higher resolution and practical application, novel experimental methods have been developed, such as high-order diffraction interference exposure, high-aspect-ratio and large-area stitching exposure, and parallel direct writing achromatic Talbot lithography. As of now, a 25 nm half-pitch pattern has been obtained; and a cm^2 exposure area has been achieved in practical samples. The above methods have been applied to extreme ultraviolet photoresist evaluation, photonic crystal and surface plasmonic effect research, and so on.

Keywords: soft x-ray, EUV, interference lithography

1. Introduction

Soft x-ray interference lithography (XIL) is a novel micro/nanoprocessing technique that utilizes the interference fringes of two or more coherent x-ray beams to expose the photoresist and obtain a periodic nanopattern [1–3]. The technique is based primarily on the third-generation synchrotron sources, of which high throughput and good coherence provide the basis for high performance XIL techniques.

[3] Authors to whom any correspondence should be addressed.

Original content from this work may be used under the terms of the Creative Commons Attribution 3.0 licence. Any further distribution of this work must maintain attribution to the author(s) and the title of the work, journal citation and DOI.

In the field of micro/nanomanufacturing, XIL is a unique parallel fabrication technique independent of mainstream extreme manufacturing techniques. It focuses on the manufacture of strictly periodic patterns. Moreover, large areas of high-resolution nanostructures can be achieved efficiently. Compared with traditional high resolution fabrication techniques [4–7], such as electron beam lithography (EBL), focused ion beam (FIB), and nanoimprint lithography (NIL), XIL has the characteristics of strict periodicity, large-area fabrication, large depth of focus, and no need for substrate conduction [8, 9]. In terms of resolution, the XIL technique's theoretical limit of resolution can reach less than 4 nm [10]. Compared with EBL and FIB, at the same resolution level, the throughput of XIL is much higher. Using XIL, the fabrication of ~ cm^2 nanostructures can be achieved within several hours. The service life of the mask and the defect control

© 2020 The Author(s). Published by IOP Publishing Ltd on behalf of the IMMT
2631-8644/20/012005+07$33.00

effect of the exposed sample are better than NIL because of the noncontact exposure method.

In extreme ultraviolet lithography (EUVL) technology, the XIL technique is used to evaluate the performance of novel extreme ultraviolet (EUV) photoresists. Soft XIL with an EUV synchrotron radiation source (EUV-IL) is a powerful tool for EUV photoresist evaluation under working conditions. Other extreme manufacturing techniques that do not use EUV light sources cannot replace its role. Moreover, on a commercial EUV lithography machine worth hundreds of millions of dollars, no manufacturer can tolerate the risk of potential contamination of the equipment by the novel photoresist. Therefore, the EUV-IL technique is currently the only feasible EUV photoresist evaluation tool.

In the Shanghai synchrotron radiation facility (SSRF), the XIL beamline (BL08U1B) applies a high brilliance undulator source and an achromatic diffraction scheme to obtain high quality interference fringes and practical throughput for a variety of scientific research and industrial applications [11]. Similarly, in the XIL-II beamline of the Swiss Light Source and BL-9 beamline of the SUBARU light source, XIL techniques have been employed in research of EUV photoresists, nanomagnetics, block copolymers, and silicon nanodevices [12–20]. The researchers in this field have ongoing efforts to develop XIL by obtaining higher exposure pattern resolution, efficiently fabricating large-area exposure patterns, and developing the exposure methods that facilitate subsequent pattern transfer [21–24]. In this article, we introduce our contributions to the above three objectives, including exposure tool optimization, new fabrication techniques, and the related applications based on these techniques.

2. The vibration condition control of the exposure system

A large number of experiments have proven that suppressing the vibration of the exposure system is the key to the success of the soft XIL experiment [25, 26]. At the XIL beamline, a laser interferometer (attocube systems AG, FPS3010) was installed on the exposure system to monitor the displacement between the mask stage and the wafer stage in the horizontal and vertical directions, thus realizing a precise real-time vibration evaluation system, as shown in figure 1. Based on this evaluation system, we determined we could monitor and further improve the stability of the exposure system and the surrounding environment and selected appropriate experimental conditions. In the current experiment, the relative position fluctuation of the mask and the sample can be controlled below 2.5 nm root mean square during a ten-minute exposure, which provides a good experimental guarantee for the subsequent XIL experiment.

3. Experimental methodologies

3.1. Interference lithography with high-order diffraction beams

The stable exposure of high-resolution patterns is the most important technical capability of the XIL beamline [27]. The XIL mask plays a key role in achieving high-quality pattern exposure. Figure 2 illustrates the basic structure of the mask grating and the principle of the dual-grating interference. The incident light is diffracted by the gratings in the mask; and the diffraction angle is set to θ, which satisfies

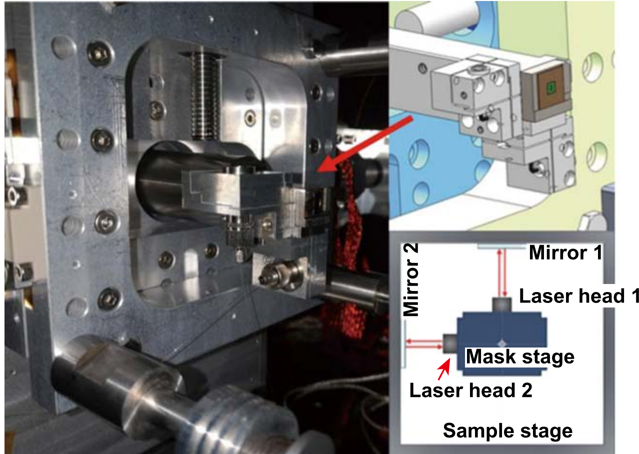

Figure 1. The schematic and experimental setup of the vibration evaluation system.

$$\sin\theta = N\lambda/P_g, \tag{1}$$

where λ is the wavelength of the incident light, P_g is the grating pitch, N is the diffraction order, and the pitch of the interference fringe is

$$P = \lambda/2\sin\theta. \tag{2}$$

Thus,

$$P = P_g/2N. \tag{3}$$

As shown by equation (3), the fringe pitch is independent of the wavelength and is only determined by the grating pitch and the diffraction order. A smaller fringe pitch can be obtained by the interference with higher order diffraction beams. At present, interference lithography based on first-order diffraction has been widely used in EUV photoresist evaluation, and interference lithography based on high-order diffraction is not widely used due to the low efficiency of mask grating, as the height and duty cycle of the grating is difficult to precisely control in the grating fabrication process [28].

Traditionally, XIL masks are first defined by EBL and then fabricated by corresponding post-processing. In the XIL-II beamline at the Swiss Light Source, a negative photoresist hydrogen silsesquioxane was adopted to form gratings directly through the EBL and obtain high-resolution exposed patterns [29], eliminating the need for cumbersome post-processing.

A set of traditional processes has been developed for the XIL masks in the SSRF XIL beamline. Furthermore, in order to meet the small pitch requirement of EUV photoresist evaluation, we have developed novel fabrication techniques that do not rely on post-processing to obtain a good quality XIL mask of smaller pitches with less line edge roughness. At present, two methods of fabricating high-order diffraction

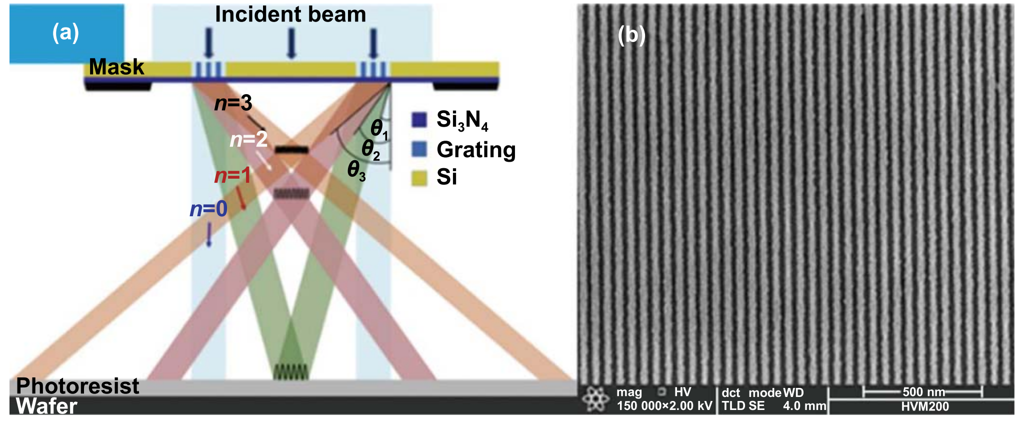

Figure 2. (a) The principle of higher order diffraction interference lithography technology and (b) the scanning electron microscopy (SEM) image of the photoresist pattern after second order diffraction interference lithography with about 25 nm half-pitch.

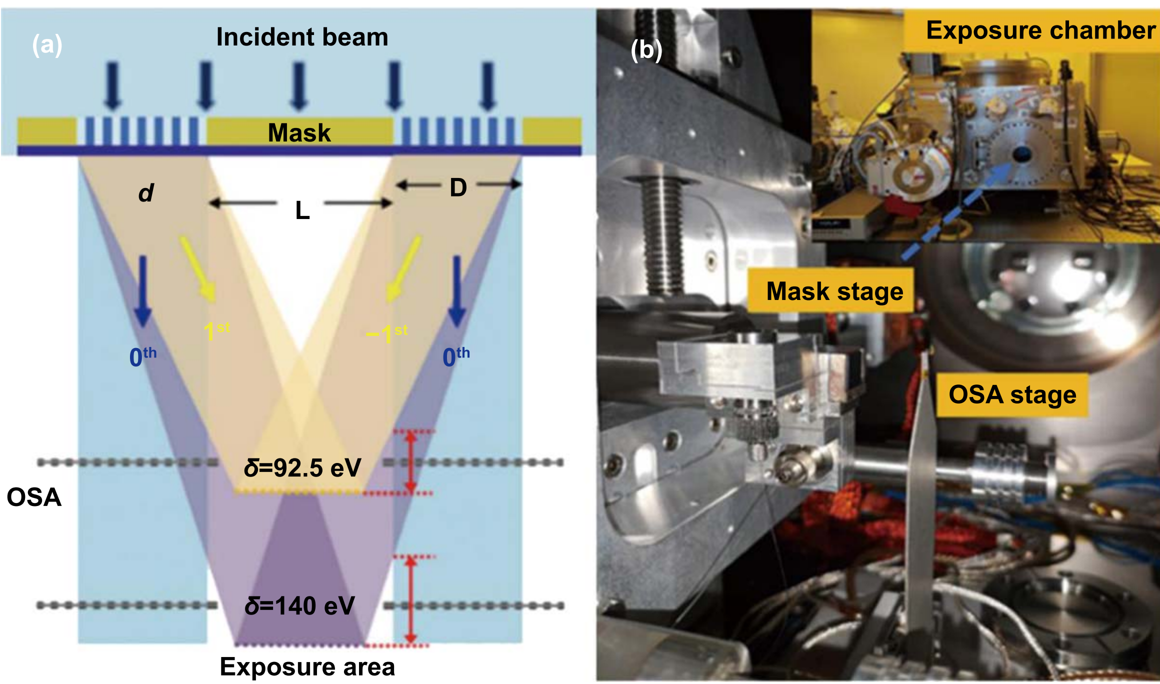

Figure 3. (a) The principle of large-area stitching deep exposure and (b) the corresponding experimental setup.

gratings have been developed. One is to fabricate gratings on the EBL-defined photoresist patterns by means of atomic layer deposition (ALD) of titanium dioxide (TiO_2) to improve the grating's diffraction efficiency, and the other is to directly fabricate the grating by the metal-oriented deposition technique without relying on EBL [30]. As shown in figure 2, nanostructures with a half-pitch of about 25 nm have been obtained by the above gratings; and these masks can work stably for a long service time under high irradiation conditions.

3.2. Large-area stitching exposure method capable of deep exposure

To satisfy the large-area sample requirements for practical micro/nanodevices and for some scientific tests [31–33], it is necessary to develop a novel XIL technique which can efficiently expose the large-area patterns with high aspect ratios. The patterns obtained by the usual XIL are determined by the pitch and arrangement of the mask gratings, and a single exposure area is determined by those of the grating. In order to accurately stitch the single-exposure fields and break the limitation of the mask grating area, we propose observing the position of the interference zone and zero-order spots on-line by a small amount of high-order harmonic x-rays before exposure and then accurately blocking the zero-order beam by an order-sorting aperture. Thus a large-area stitching technique has been developed in the SSRF XIL beamline [34]. The principle and experimental setup are shown in figure 3. Using this technique, the zero-order spots around the interference pattern were eliminated; and thus a large-area pattern was obtained with

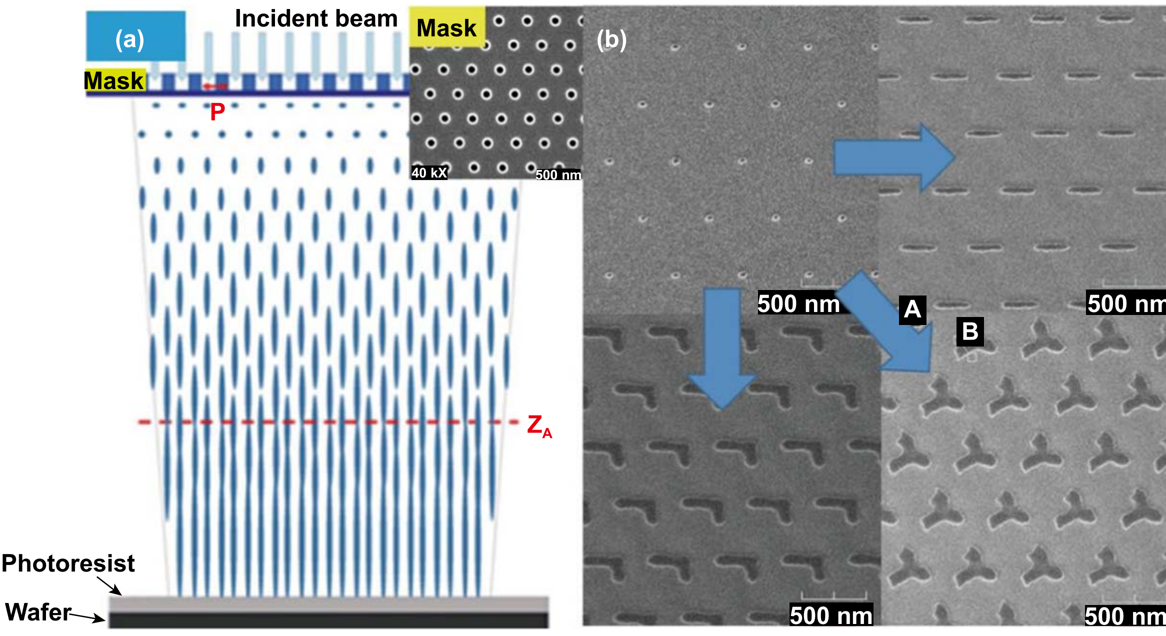

Figure 4. (a) The principle of achromatic Talbot lithography (ATL) and an ATL mask consists of a hexagonal chromium (Cr) lattice with a 520 nm pitch and 130 nm hole diameter. (b) A 520 nm pitch lattice with a spot diameter of approximately 50 nm obtained directly from ATL, and further complex patterns obtained by direct writing achromatic Talbot lithography (DW-ATL) scanning.

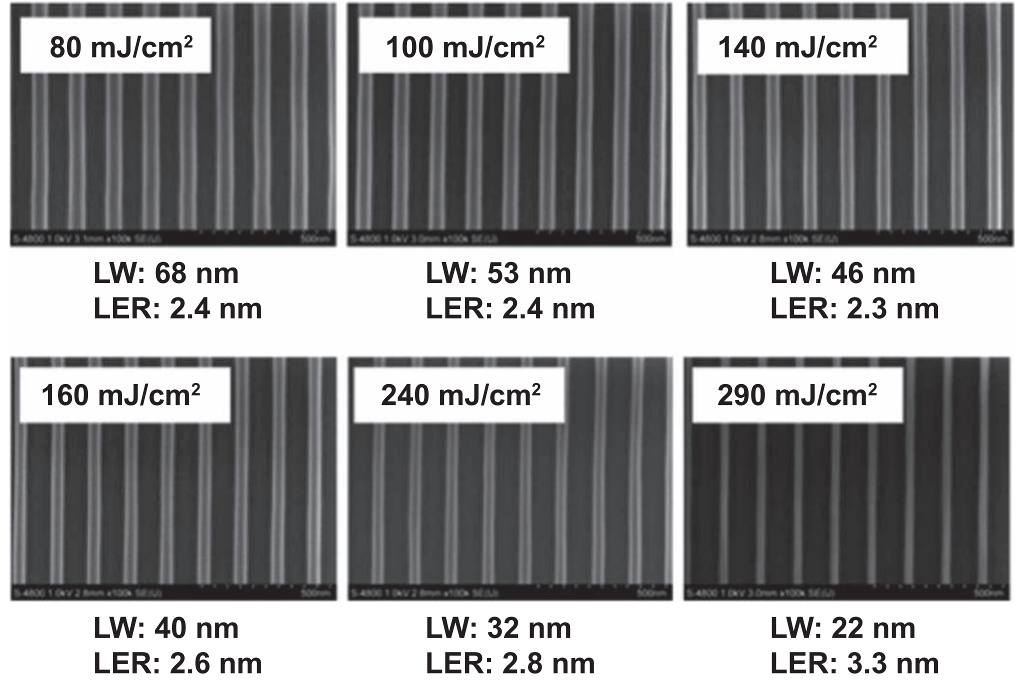

Figure 5. High-resolution scanning electron microscopy (SEM) images of line-space patterns (top view) for various exposure doses, with line width (LW) and line-edge roughness (LER) values. It was performed at SSRF with a grating period of 280 nm and a pattern period of 140 nm. Reprinted with permission from [49]. Copyright 2019 American Chemical Society.

micron precision stitching. In order to achieve high aspect ratio patterns, an incident light was selected with a photon energy 140 eV, higher than the usual 92.5 eV. Thus, a set of masks with permalloy blocking layers was developed to deal with the higher photon energy [35]. Patterns with an aspect ratio of up to 3 at 100 nm half-pitch were achieved using this fabrication process. Combining the above two methods, we further obtained a large-area (1.44 cm^2), nanoperiodic structure with an aspect ratio of 3 [36] and achieved pattern transfer using different processes, such as etching and lift-off. In order to meet the demands of different applications, we have successfully fabricated nanostructures on different substrates, such as silicon (Si), yttrium aluminum garnet (YAG), and silicon dioxide (SiO_2).

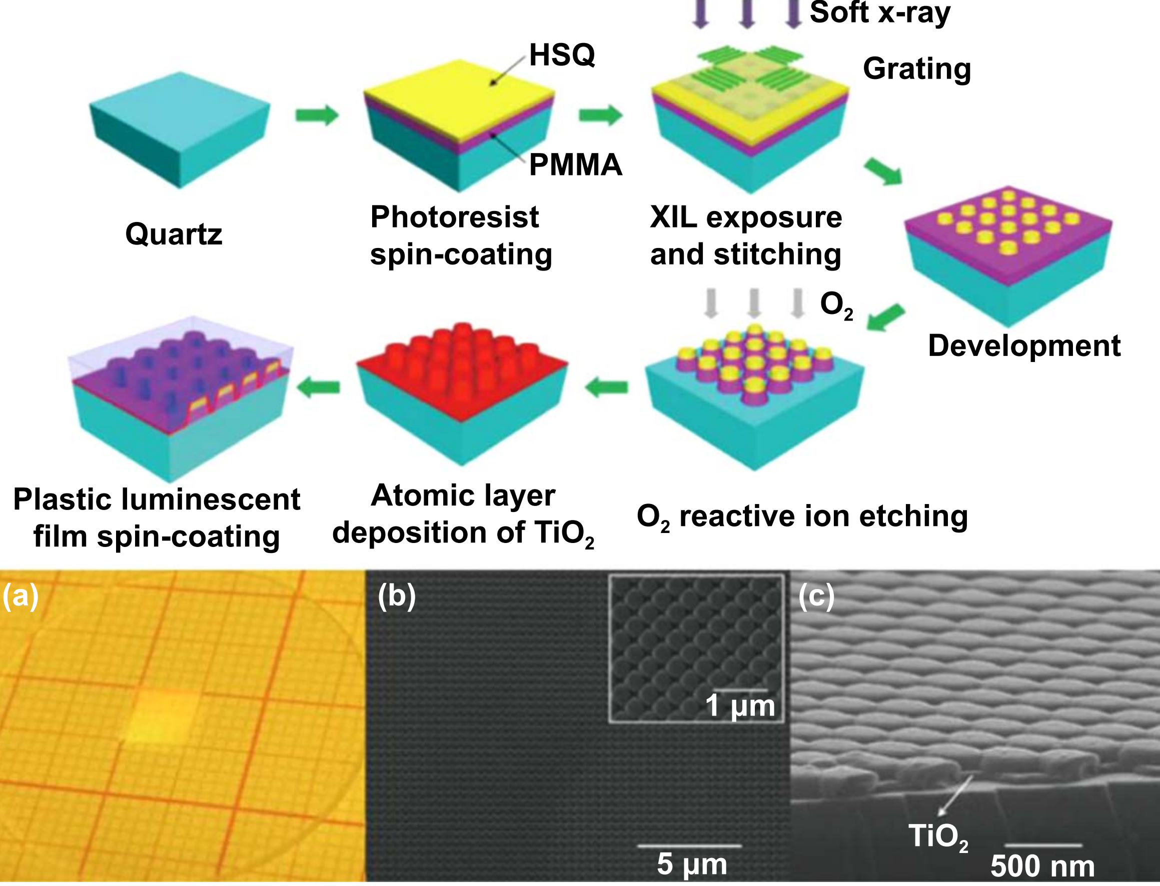

Figure 6. Schematic illustration of the fabrication process of the two-dimensional crystal structures coated with plastic luminescent films and the sample fabricated by this process. Reproduced from [53]. CC BY 4.0.

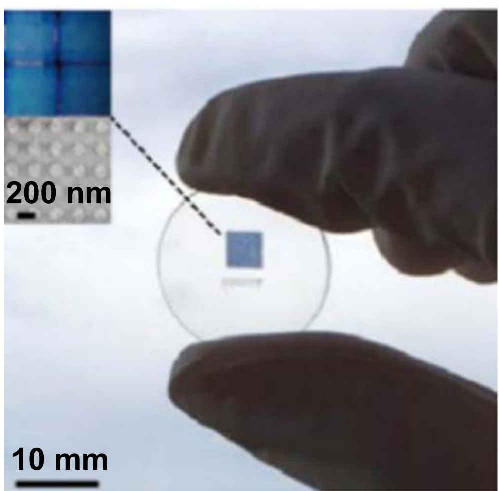

Figure 7. Nanostructured filters fabricated by stitching x-ray interference lithography (XIL), consisting of nanocylinders on a 20 nm thick Ag film. Reproduced from [57]. CC BY 4.0.

3.3. Parallel direct writing achromatic Talbot lithography (ATL)

Periodic structures with complex cells can be widely applied to various research fields, such as the polarization adjustment of light, large-area magnetic recording elements, and full absorption modulation of broadband light [37–39]. However, the normal XIL technique can only fabricate the nanoarrays with simple lines or dots. For this reason, a parallel direct writing achromatic Talbot lithography (DW-ATL) was developed for the complex structures in the above applications [40, 41]. The principle and preliminary experimental results of DW-ATL are shown in figure 4. The light spot arrays obtained by ATL are employed as the basic exposure units. Periodic patterns with complex cells can be achieved by scanning the wafer stage with nanometer precision. The scanning accuracy is controlled through the laser interferometer feedback during the exposure. Periodic nanostructures with a resolution 60 nm were fabricated, with short-line, L-shaped, and tri-shaped cells.

4. Applications

4.1. EUV photoresist evaluation

EUVL is a candidate for large-scale integrated circuits moving toward 7 nm and below process nodes, and EUV photoresist is considered to be one of the most important key techniques for EUVL [42, 43]. Due to the high cost of EUVL tools and the high risk of damage to EUV tools' internal environment, it is unrealistic to use EUVL tools for EUV photoresist evaluation during development. EUV interference lithography based on a 92.5 eV synchrotron radiation source

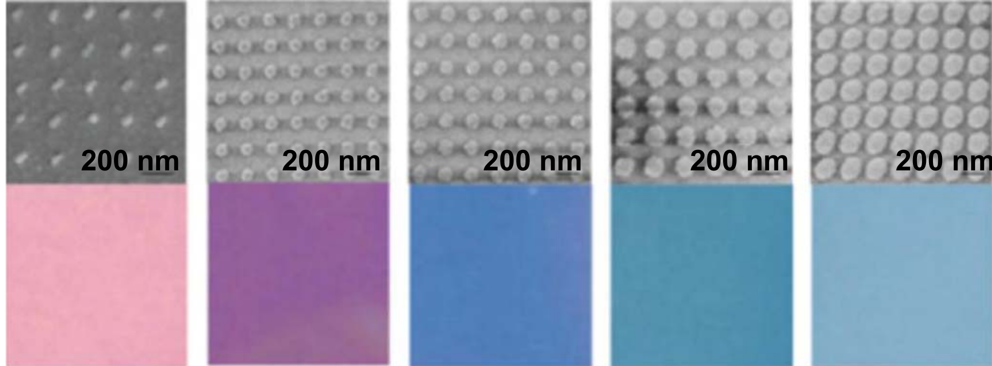

Figure 8. Different nanostructures and corresponding filter characteristics. The structure pitch is 230 nm and the fill factor is from 0.25 to 0.75. Reproduced from [57]. CC BY 4.0.

is recognized as the most effective EUV photoresist evaluation tool [44–47], which can greatly accelerate the development of EUV photoresists. The XIL beamline at SSRF has established a complete evaluation platform for EUV photoresist sensitivity, resolution, line edge roughness, and outgassing analysis [48]. A large amount of EUV photoresist research work has been conducted based on the platform, and figure 5 shows the EUV photoresist test results [49].

4.2. Scintillator extraction efficiency enhancement

A scintillator plays an important role in radiation detection systems and has various applications in high-energy physics experiments and nuclear medicine imaging [50–52]. The efficiency of a scintillator-based detector is highly dependent on luminescence conversion efficiency and light extraction efficiency. At present, a large-area stitching exposure XIL technique is applied to fabricate nanoscale periodic structures on scintillators to improve light extraction efficiency.

For example, the photonic crystal structures fabricated on the surface of a BGO scintillator using a combination of XIL with ALD [53], as shown in figure 6, can achieve significantly enhanced light extraction based on the outcoupling of the evanescent field with the photonic crystal structures. A 95.1% enhancement was obtained in the present study. A high refractive index due to the conformal TiO_2 layer enables the efficient coupling and thus the enhanced extraction efficiency with a relatively low height of the structured layer. This method is very promising for light extraction of devices in which a large-area surface is required for practical applications.

4.3. Optical filtering

Surface plasmons (SP) have become the focus of various fields due to their extraordinary ability to manipulate light beyond the optical diffraction limits [54–56]. As shown in figures 7 and 8, the large area stitching exposure XIL technique has played an important role in SP-based plasma color filter research [57, 58].

5. Conclusions

In the field of micro/nanomanufacturing, XIL is a unique parallel fabrication technique independent of mainstream extreme manufacturing techniques. Large areas of high-resolution, strictly periodic nanostructures can be achieved efficiently by this technique. As the only feasible tool for novel EUV photoresist evaluation, the EUV-IL technique plays an important role in EUVL technology. A precise real-time vibration evaluation system has been established in the SSRF XIL beamline to suppress the vibration sources and ensure the stability of the exposure process. On this basis, novel XIL techniques have been developed, such as high-order diffraction XIL exposure, deep XIL exposure, large-area stitching exposure, and parallel DW-ATL. At present, photoresist patterns of 25 nm half-pitch, cm^2 exposure area, and an aspect ratio of 3 have been achieved. Based on these new methods, many applications have been carried out, such as EUV photoresist performance testing, photonic crystal preparation, and SP effect devices.

Acknowledgments

This work was performed at the SSRF XIL beamline (BL08U1B). Financial support was provided by the National Key R&D Program of China (2017YFA0206001), the National Key Basic Research Program of the China Science and Technology Commission of Shanghai Municipality (17JC1400802), and the National Natural Science Foundation of China (Nos. 11775291, 11875314).

ORCID iDs

Jun Zhao https://orcid.org/0000-0002-7692-1178
Shumin Yang https://orcid.org/0000-0003-3297-8444
Zhaofeng Liang https://orcid.org/0000-0003-4597-1487
Yanqing Wu https://orcid.org/0000-0001-7684-892X

References

[1] Harun H S, David C, Gobrecht J, Golovkina V, Cerrina F, Kim S O and Nealey P F 2003 *Microelectron. Eng.* **67–8** 56–62
[2] Harun H S 2005 *Microelectron. Eng.* **78-79** 410–6
[3] Nassir M, Daniel F, Jens G and Yasin E 2014 *Opt. Lett.* **39** 2286–9
[4] Zhengjun L, Kari I, Nikolai C, Kestutis G and Ilkka T 2013 *Nanotechnology* **24** 175304
[5] Li H, Ye T, Shi L and Xie C 2017 *J. Micromech. Microeng.* **27** 124002
[6] Xie C, Zhu X, Niu J, Li H, Liu M, Chen B, Hu Y and Shi L 2011 *Acta Opt. Sin.* **31** 0900128
[7] Chao W, Keith J M, Zengli F, Wen-Di L and Stephen Y C 2011 *Nanotechnology* **22** 445301
[8] Wang L, Harun H S and Yasin E 2012 *Nanotechnology* **23** 305303
[9] Nassir M, Jens. G and Yasin E 2015 *Microelectron. Eng.* **143** 55–63
[10] Birgit P, Andreas L, Eugenie K, Christian D and Yasin E 2011 *Nanotechnology* **22** 37
[11] Yang S M, Wang L S, Zhao J, Xue C F, Liu H G, Xu Z J, Wu Y Q and Tai R Z 2015 *Nucl. Sci. Tech.* **26** 010101
[12] Vaida A *et al* 2009 *J. Micro/Nanolith. Mems Moems* **8** 021204
[13] Matthias D, Tugce N G, Amitav S, Nicholas D S and Celestino P 2015 *ACS Appl. Mater. Interfaces* **7** 11337–45
[14] Yasuyuki F, Yuya Y, Takafumi I, Takuro U, Tetsuo H, Takeo W and Kinoshita H 2011 *Microelectron. Eng.* **88** 1944–7
[15] Zuhal T, Michaela V, Iacopo M, Karen G O, Marieke M, Oktay Y, Rik H, Gijsbert R, Rolf C and Yasin E 2018 *Proc. SPIE* **10583** 105831W
[16] Roel G, Harun H S, Yasin E, Amandine J and Frieda V R 2006 *Microelectron. Eng.* **83** 1103–6
[17] Daniel F, Hans S, Ralph S and Yasin E 2017 *Phys. Rev.* B **96** 115307
[18] Yogesh J, Shankar K J, Mario A, Jörg F L and Yasin E 2007 *Nat. Photon.* **1** 41
[19] Hideaki T, Shinji T, Toru F, Hiroo T and Takahiro G 2014 *Proc. SPIE* **9048** 90481E
[20] John W, Cheng Y C, Artak I, Quinn L, Mike F, Mike G, Joseph B, Paul N and Franco C 2007 *Nucl. Instrum. Methods Phys. Res.* A **582** 254–7
[21] Yasin E, Harun H S, Celestino P, Jens G, Mark P S and Paul F N 2007 *Microelectron. Eng.* **84** 700–4
[22] Jintang H, Daniel F, Yasin E and Celestino P 2015 *Microelectron. Eng.* **141** 32–6
[23] Waiz K, Simon A T, Mehtap O, Thomas J S, Jens G, Jeroen A B and Yasin E 2015 *Nanoscale* **7** 7386
[24] Yasin E, Michaela V, Nassir M and Daniel F 2014 *Proc. SPIE* **9048** 904804
[25] Urayama T, Watanabe T, Yamaguchi Y, Matsuda N, Fukushima Y, Iguchi T, Harada T and Kinoshita H 2011 *J. Photopolymer Sci. Technol.* **24** 153–7
[26] Lin C H, Fong C H, Lin Y M, Lee Y Y, Fung H S and Shew B Y 2011 *Microelectron. Eng.* **88** 2639–43
[27] Lin C H, Lin Y M, Liang C C, Lee Y Y, Fung H S, Shew B Y and Chen S H 2012 *Microelectron. Eng.* **98** 194–7
[28] Artak I, Wüest A, John W, Fan J and Franco C 2016 *Opt. Express* **16** 9106
[29] Mojarad N, Hojeij M, Wang L, Gobrecht J and Ekinci Y 2015 *Nanoscale* **7** 4031
[30] Meijer T, Beardmore J P, Fabrie C G C H M, van Lieshout J P, Notermans R P M J W, Sang R T, Vredenbregt E J D and van Leeuwen K A H 2011 *Appl. Phys.* B **105** 703–13
[31] Wang L, Solak H and Ekinci Y 2012 *Nanotechnology* **23** 305303
[32] Pingping Z, Shumin Y, Liansheng W, Jun Z, Zhichao Z, Bo L, Jun Z and Xuhui S 2014 *Nanotechnology* **25** 245301
[33] Parisse P, Luciani D, D'Angelo A, Santucci S, Zuppella P, Tucceri P, Reale A and Ottaviano L 2009 *Mater. Sci. Eng.* B **165** 227–30
[34] Chaofan X, Yanqing W, Fangyuan Z, Shumin Y, Haigang L, Jun Z, Liansheng W and Renzhong T 2016 *Rev. Sci. Instrum.* **87** 043303
[35] Jun Z, Yanqing W, Chaofan X, Shumin Y, Liansheng W, Fangyuan Z, Zhichao Z, Bo L, Yong W and Renzhong T 2017 *Microelectron. Eng.* **170** 49–53
[36] Chaofan X *et al* 2017 *Appl. Surf. Sci.* **425** 553–7
[37] Birgit P, Hannes M, Reto G, Luca B, Sergey G, Christian D, Jorg F L, Thomas F and Yasin E 2011 *Acs Nano* **5** 6374–82
[38] Zhang X, Deng R, Yang F, Jiang C, Xu S and Li M 2018 *ACS. Photonics* **5** 2997–3002
[39] Li Z, Butun S and Aydin K 2014 *ACS Nano* **8** 8242–8
[40] Shumin Y, Chaofan X, Jun Z, Liansheng W, Yanqing W and Renzhong T 2019 *Nanotechnology* **30** 315301
[41] Huijuan X, Shumin Y, Liansheng W, Jun Z, Chaofan X, Yanqing W and Renzhong T 2019 *Chin. Opt. Lett.* **17** 062201
[42] Li L, Liu X, Pal S, Wang S L, Ober C K and Giannelis E P 2017 *Soc. Rev.* **46** 4855–66
[43] Allen R D, Thackeray J W and Somervell M H 2011 *Proc. SPIE* **7972** 797204
[44] Tomoki N *et al* 2016 *J. Photopolymer Sci. Technol.* **29** 475–8
[45] Carmen P, Andreas F, Alexandra M, John R, Yasin E and Alex P G 2017 *SPIE Adv. Lithography* **10143** 101430V
[46] Yildirim O *et al* 2017 *SPIE Adv. Lithography* **10143** 101430Q
[47] Zuhal T, Xiaolong W, Iacopo M, Lidia van Lent P, Marieke M, Rolf C, Gijsbert R, Rik H and Ekinci Y 2018 *Proc. SPIE* **10809** 108090L
[48] Li C *et al* 2014 *Sci. China Chem.* **57** 1746–50
[49] Jinping C *et al* 2019 *ACS Appl. Polym. Mater.* **1** 526–34
[50] Zhichao Z *et al* 2017 *Appl. Phys. Lett.* **110** 051901
[51] Zhichao Z *et al* 2015 *Appl. Phys. Lett.* **106** 241901
[52] Shuang W *et al* 2016 *Opt. Express* **24** 231
[53] Qiang W, Bo L, Zhichao Z, Mu G, Hong C, Chaofan X, Jun Z, Yanqing W, Renzhong T and Xiaoping O 2018 *Sci. Rep.* **8** 9254
[54] Xiaolin H *et al* 2016 *Appl. Opt.* **55** 148–52
[55] Ming Y *et al* 2015 *J. Alloys Compd.* **621** 244–9
[56] Xiaolin *et al* 2017 *J. Appl. Phys.* **121** 153105
[57] Libin S *et al* 2016 *Opt. Express* **24** 19112
[58] Qingjun W *et al* 2019 *Opt. Lett.* **44** 1031